Combescure *Advanced Modeling and Simulation in Engineering Sciences* 2014, **1**:2
http://www.amses-journal.com/content/1/1/2

Advanced Modeling and Simulation in Engineering Sciences
a SpringerOpen Journal

RESEARCH ARTICLE Open Access

Modeling elastic-plastic buckling of sandwich axisymmetric shells: on the limits of "shell" models and analytical solutions

Alain G Combescure

Correspondence:
alain.combescure@insa-lyon.fr
LaMCoS, INSA-Lyon, Université de Lyon, CNRS UMR 5259, 18-20 rue des Sciences, F69621 Villeurbanne, France

Abstract

Background: The objective of this paper is to answer the question: "Can a 'shell' model always be used to predict the elastic buckling of a shell?"

Method: This paper shows that such a model leads to significantly overestimated critical loads in the case of sandwich shells and gives an explanation for this overestimation.

Results: A dependable model is proposed and applied to a few structures of revolution, for which it is shown that shell analyses are sometimes overly on the unsafe side.

Conclusion: Of course, in such cases, 3D analysis is possible, but the associated computation cost is several orders of magnitude higher than that of the Fourier series analysis proposed in this paper.

Background

Computational modeling techniques to analyze the buckling of anisotropic and multilayered shells are very well developed, so that further advances may not seem necessary. However the quest for lighter structures, which has induced many studies for decades, has led to the development of sandwich structures in order to manufacture robust, yet lightweight, mechanical parts. Some of these parts are subjected to compression and their buckling strength must be assessed. The prediction of the critical buckling loads of these structures seems to be simple: it suffices to model these objects as multilayered shells, thus leading to an immediate prediction of their critical loads. However, a comparison of the critical loads predicted from calculations with experimental results reveals significant differences. Some remarkable works on buckling [1-3] were published at the turn of the century, and quasi-analytical solutions have been proposed for cylinders in axial compression [4]. These solutions take into account two types of buckling: global shell buckling and local skin buckling (wrinkling). Many works dealing with the study of crashworthiness optimization (e.g. [5-7]) are also available. Some authors have also worked on the interaction between the two types of buckling [8-11] and shown that in some cases this interaction leads to a critical load which is smaller than that predicted by calculating the critical loads of each mode independently. The objective of the present work is to examine the finite element modeling of this problem in the case of axisymmetric structures and propose a modeling strategy which leads to good results in all situations. The particular case of plastic buckling is also analyzed in depth.

The paper is structured as follows:

- first, the modeling of elastic-plastic buckling and its application to structures of revolution is reviewed;
- then, three sample applications are presented(a cone under internal pressure, a cone under external pressure, and a sphere under external pressure).

Method : A short review of the modeling of the elastic-plastic buckling of structures of revolution

Elastic buckling of structures of revolution

The structures being considered in this work are structures of revolution subjected to axisymmetric loading. Their elastic response (which can involve geometric and material nonlinearities) is also axisymmetric. However, when studying the stability of these objects, the loss of this symmetry of revolution must be envisaged. Because of the axisymmetric nature of both the structure and the constraints, the instability mode can be decomposed into a Fourier series. One can easily show (Koiter [12], Bushnell [13,14]) that in the case of a perfectly axisymmetric structure subjected to axisymmetric loading the instability involves only a single Fourier mode. This type of problem can be modeled using axisymmetric finite elements and a Fourier series decomposition. This is the chosen approach because it is quite efficient. 3D shells, or even solid elements, could also be used, but these would lead to much longer computation times. Two means of modeling these sandwich shells will be compared: the multilayer shell model called COQMULT, whose kinematics requires that the distance between layers remain constant during the deformation, and an axisymmetric volume model denoted QUA8 (in our case, an 8-node element enabling an exact representation of a linearly varying strain across the thickness), which removes all kinematic constraints between the two skins. Let us consider the local coordinate system s, θ, n which is tangent to the shell at any point of the mid-surface (Figure 1).

The membrane strains ϵ_{ij}^m and bending strains ϵ_{ij}^b for shells are well-known [15,16]. They are recalled below in the case of the Kirchhoff-Love theory for the n^{th} Fourier mode:

$$\epsilon_{ss}^m = \frac{\partial u}{\partial s} - \frac{w}{R} \tag{1}$$

$$\epsilon_{\theta\theta}^m = \frac{1}{r}\left(\frac{\partial v}{\partial \theta} + w\, cos\phi + u\, sin\phi\right) \tag{2}$$

$$\epsilon_{s\theta}^m = \frac{1}{2}\left(\frac{\partial v}{\partial s} + \frac{1}{r}\left(\frac{\partial u}{\partial \theta} - v\, sin\phi\right)\right) \tag{3}$$

$$\epsilon_{ss}^b = -\frac{\partial^2 w}{\partial s^2} - \frac{1}{R}\frac{\partial u}{\partial s} \tag{4}$$

$$\epsilon_{\theta\theta}^b = \frac{1}{r^2}\left(-\frac{\partial^2 w}{\partial \theta^2} - r\, sin\phi\frac{\partial w}{\partial s} + cos\phi\frac{\partial v}{\partial \theta} - \frac{r}{R}u\, sin\phi\right) \tag{5}$$

$$\epsilon_{s\theta}^b = \frac{1}{2r^2}\left(-2r\frac{\partial^2 w}{\partial s \partial \theta} + 2r\, cos\phi\frac{\partial v}{\partial s} - \frac{r}{R}\frac{\partial u}{\partial \theta} - v\, sin\phi\, cos\phi + \frac{\partial w}{\partial \theta}sin\phi\right) \tag{6}$$

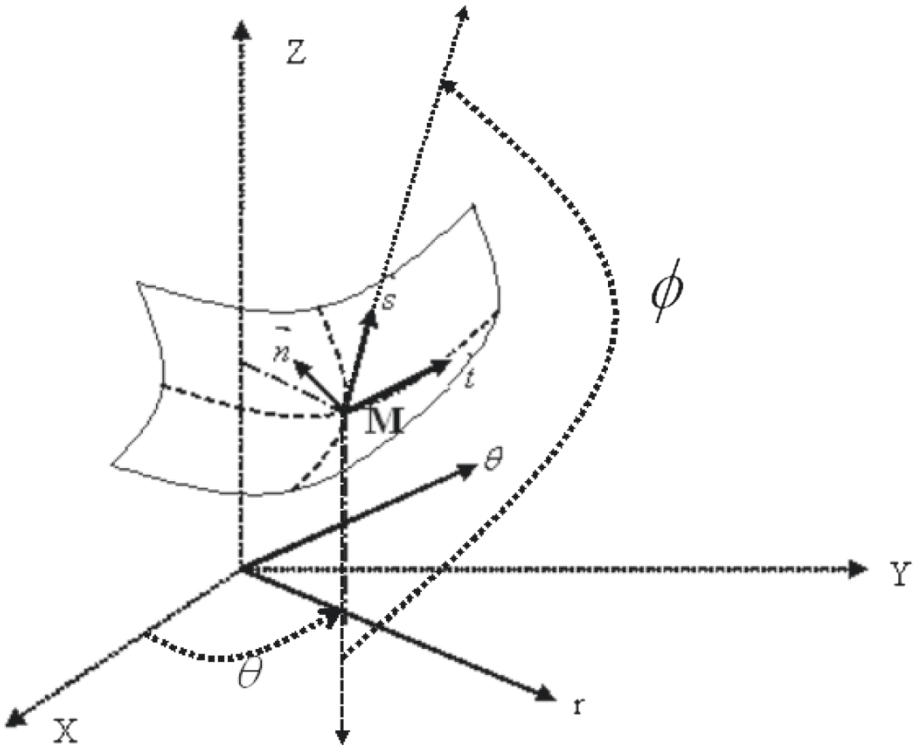

Figure 1 Definition of the local coordinate system for an axisymmetric shell.

where u, v, w denote respectively the axial, circumferential and normal displacements of the shell. r is the distance to the axis of revolution, R the axial curvature of the shell, and ϕ the angle with direction $-z$ ($+z$ being the axis of revolution).

The quadratic membrane strains , which measure the variation of the shell strain state in an infinitely small increment, and thus enable one to calculate buckling are given by:

$$\epsilon_{ss}^{q} = \frac{1}{2}\left[\left(\frac{\partial w}{\partial s} + \frac{u}{R}\right)^2 + \left(\frac{\partial u}{\partial s} - \frac{w}{R}\right)^2 + \left(\frac{\partial v}{\partial s}\right)^2\right] \tag{7}$$

$$\epsilon_{\theta\theta}^{q} = \frac{1}{2r^2}\left[\lambda_\phi^2 + \mu_\phi^2 + \eta_\phi^2\right] \tag{8}$$

$$\epsilon_{s\theta}^{q} = \frac{1}{2r}\left[\lambda_\phi\left(\frac{\partial w}{\partial s} + \frac{u}{R}\right) + \left(\frac{\partial u}{\partial s} - \frac{w}{R}\right)\mu_\phi + \frac{\partial v}{\partial s}\eta_\phi\right] \tag{9}$$

where $\lambda_\phi = \frac{\partial w}{\partial \theta} - v cos\phi$, $\mu_\phi = \frac{\partial u}{\partial \theta} - v sin\phi$ and $\eta_\phi = \frac{\partial v}{\partial \theta} + w cos\phi + u sin\phi$. For the volume elements ($QUA8$), the linear strains are:

$$\epsilon_{rr} = \frac{\partial u_r}{\partial r} \tag{10}$$

$$\epsilon_{zz} = \frac{\partial u_z}{\partial z} \tag{11}$$

$$\epsilon_{\theta\theta} = \frac{1}{r}\left(u_r + \frac{\partial v}{\partial \theta}\right) \tag{12}$$

$$\epsilon_{rz} = \frac{1}{2}\left(\frac{\partial u_r}{\partial z} + \frac{\partial u_z}{\partial r}\right) \tag{13}$$

$$\epsilon_{r\theta} = \frac{1}{2}\left(\frac{\partial v}{\partial r} + \frac{1}{r}\left(\frac{\partial u_r}{\partial \theta} - v\right)\right) \tag{14}$$

$$\epsilon_{z\theta} = \frac{1}{2}\left(\frac{\partial v}{\partial z} + \frac{1}{r}\frac{\partial u_z}{\partial \theta}\right) \tag{15}$$

In these expressions, u_r, u_z, v denote respectively the radial displacement, the vertical displacement and the circumferential displacement. The quadratic strains are:

$$\epsilon^q_{rr} = \left[\left(\frac{\partial u_r}{\partial r}\right)^2 + \left(\frac{\partial u_z}{\partial r}\right)^2 \left(\frac{\partial v}{\partial r}\right)^2\right] \tag{16}$$

$$\epsilon^q_{zz} = \left[\left(\frac{\partial u_r}{\partial z}\right)^2 + \left(\frac{\partial u_z}{\partial z}\right)^2 \left(\frac{\partial v}{\partial z}\right)^2\right] \tag{17}$$

$$\epsilon^q_{\theta\theta} = \frac{1}{r^2}\left[\left(\frac{\partial u_r}{\partial \theta} - v\right)^2 + \left(\frac{\partial u_z}{\partial \theta}\right)^2 + \left(u_r + \frac{\partial v}{\partial \theta}\right)^2\right] \tag{18}$$

$$\epsilon^q_{rz} = \frac{1}{2}\left(\frac{\partial u_r}{\partial r}\frac{\partial u_r}{\partial z} + \frac{\partial u_z}{\partial r}\frac{\partial u_z}{\partial z} + \frac{\partial v}{\partial r}\frac{\partial v}{\partial z}\right) \tag{19}$$

$$\epsilon^q_{r\theta} = \frac{1}{2r}\left[\left(\frac{\partial u_r}{\partial \theta} - v\right)\frac{\partial u_r}{\partial r} + \frac{\partial u_z}{\partial \theta}\frac{\partial u_z}{\partial r} + \left(\frac{\partial v}{\partial \theta} + u_r\right)\frac{\partial v}{\partial r}\right] \tag{20}$$

$$\epsilon^q_{z\theta} = \frac{1}{2r}\left[\left(\frac{\partial u_r}{\partial \theta} - v\right)\frac{\partial u_r}{\partial z} + \frac{\partial u_z}{\partial \theta}\frac{\partial u_z}{\partial z} + \left(\frac{\partial v}{\partial \theta} + u_r\right)\frac{\partial v}{\partial z}\right] \tag{21}$$

Finally, buckling analysis consists of two steps: first the calculation of the axisymmetric prestress and then a series of buckling calculations for each Fourier mode j. The critical load and the associated critical mode correspond to the Fourier mode j which leads to the smallest load.

The shell finite elements chosen for the calculations are plane shell elements ($\frac{1}{R} = 0$) which possess only four degrees of freedom per node (three translations plus the rotation about the circumferential direction) [15].

The volume elements chosen are 8-node isoparametric axisymmetric elements with three Fourier degrees of freedom.

Nonlinear buckling of structures of revolution

Nonlinear instability may develop in any non linear analysis: for a given load level, they are characterized by the existence of more than one equilibrium state. For an axisymmetric structure the unstable state can be either axisymmetric or non-axisymmetric. If the structure remains axisymmetric, well-known incremental calculation techniques with control (such as the arc-length control method [17,18]) can generally be used to predict

the critical load, except when the loading is exactly orthogonal to the instability mode. However, if the instability mode is not axisymmetric, this instability cannot be predicted using incremental analysis alone. In that case, there are two possible modeling strategies for predicting instability.

- The first strategy consists in meshing the structure of revolution in 3D and using this mesh to seek the instability. However, one should note that if the mesh satisfies the symmetry of revolution and the loading is axisymmetric the 3D analysis leads to an axisymmetric deformed shape and, thus, "misses" the non-axisymmetric instability. In this case, one must either introduce a defect (by perturbing the mesh of the structure or the loading) or use a mesh which does not satisfy the symmetry of revolution, hoping that this "imperfection" will solicit the instability sufficiently for it to develop "naturally."
  One can also use the specific technique of axisymmetric elements with non-axisymmetric defects ([16,19]).
- The second strategy consists in calculating the nonlinear response of the structure of revolution (which, thus, remains axisymmetric), then checking the stability of each resulting nonlinear state k. In such a stability study, for each load step k, one examines all the possible Fourier modes: the instability point is the first step k whose load multiplier is equal to 1. This Fourier analysis with uncoupled modes is still possible even though the response of the structure is nonlinear (in terms of geometry or material) because the preloads remain axisymmetric.

The geometrically nonlinear case

In the case of a pure geometrically nonlinear response, one calculates the axisymmetric equilibrium states using standard nonlinear incremental techniques. Thus, one obtains a sequence of m equilibrium states, denoted C_k, which are characterized by two variable fields: the displacement field between the initial structure and the current structure u_k, and the equilibrated Cauchy stress field σ_k. Once these m states have been found, one studies their stability. In order to do that, one calculates the stability of the deformed shape which corresponds to each state C_k by examining all the possible Fourier modes to find the mode j which leads to the smallest critical load λ_j^k. The first state k which satisfies $\lambda_j^k = 1$ is the critical state: then, buckling occurs following Fourier mode j. One should stress the fact that this buckling is usually associated with a loss of symmetry of revolution (if $j \neq 0$).

The elastic-plastic case

In this case, modeling the instability is a little trickier because of the unilateral nature of the elastic-plastic constitutive relation. The calculation of the equilibrium states follows the same scheme as in the geometrically nonlinear case: one calculates a sequence of statically and plastically admissible states, again denoted C_k. These states are characterized by three quantities: the displacements and stresses (as in elasticity), plus the internal variables A_k. One shall now consider the special case of Von Mises elastic-plastic case, but the present approach is the same for any irreversible elastic-plastic material. In case of damage model, this procedure is still valid but must be applied in a slightly modified manner. Let us consider the case of a tension curve

with Young's modulus E, tangent modulus E_T and secant modulus E_s, as shown in Figure 2 below.

In order to calculate the instability using the same method as in nonlinear elasticity, one must linearize the constitutive relation during the buckling around state C_k. The natural way to linearize the material's behavior around the current state is simply to use the tangent constitutive law for all Gauss points on the loading surface, *i.e.* to consider the tangent constitutive equation:

$$\underline{\underline{H_t}} = \underline{\underline{H}} \left(\underline{\underline{I}} - \frac{\underline{\underline{A}} \left[\underline{s} \otimes \underline{s}^T \right] \underline{\underline{AH}}}{s^{*2} E_h + \underline{s}^T \underline{\underline{AHA}} \underline{s}} \right) \tag{22}$$

In this equation, H is the elastic constitutive matrix, s the stress deviator and E_h the elastic-plastic slope, which is related to the tangent modulus through the equation:

$$E_h = \frac{E\, E_T}{E - E_T} \tag{23}$$

s^* is Von Mises' equivalent stress. A, the operator which leads to Von Mises' stress knowing the components of the tensor, is given by the relation:

$$s^* = \sqrt{\underline{\sigma}^T \underline{\underline{A}} \underline{\sigma}} \tag{24}$$

Thus, the equilibrium states can be calculated incrementally. When the loading increases monotonically, the iterations converge rapidly. In the case of unloading, or when the direction of loading changes abruptly, the increment in the local stress tensor is very different from the current state and this tangent behavior operator, which is calculated using one's knowledge of the current stress state, is far from predicting the correct increment. For example, if one considers a stress state over the loading surface and the stress increment is tangent to the plasticity convex set, this approach leads to an elas-

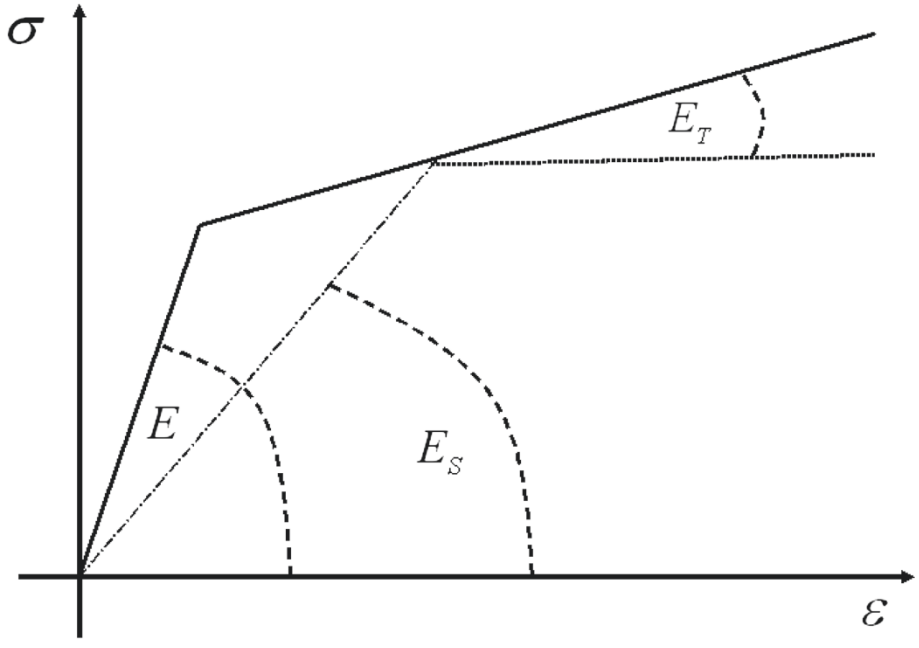

Figure 2 The stress-strain curve and definition of the different moduli.

tic increment. In the case of incremental analyses, this approximation is corrected by the constraint that the final state must be plastically admissible. This remark shows that if one evaluates the stability of a state using for state C_k the standard tangent constitutive matrix based on incremental plasticity theory (which is what is done in most programs) one tends to overestimate the stiffness, which leads to an unsafe prediction of the instability. This is an unconservative method of predicting plastic instability. The most pessimistic approximation consists, for any stress state on the plasticity convex set, in choosing the approximation of the tangent modulus which uses the following equation for the tangent constitutive matrix:

$$\underline{\underline{H_t}} = \frac{E_T}{E}\underline{\underline{H}} \tag{25}$$

The middle-of-the-road method consists in using finite plasticity theory, in which, at any point of the loading surface, the tangent constitutive law is approximated by Equation 26. These three ways of calculating the tangent stiffness in buckling can be applied in the general case, whether one uses a COQMULT model or a QUA8 continuum mechanics model.

$$\underline{\underline{H_t}} = \left[\left(\frac{1}{E_T} - \frac{1}{E_S}\right)\frac{\underline{\underline{A}}\underline{s} \otimes \underline{s}^T\underline{\underline{A}}}{s^{*2}} + \underline{\underline{H}}^{-1} + \left(\frac{1}{E_S} - \frac{1}{E}\right)\underline{\underline{A}}\right]^{-1} \tag{26}$$

Results and discussions

Now let us apply the buckling models to the prediction of elastic and elastic-plastic buckling for three types of sandwich shells:

- a half-sphere fixed at the base and subjected to uniform external pressure;
- three cone frustra fixed at their bases and subjected to uniform external pressure;
- the same three cone frustra, this time subjected to uniform internal pressure.

Geometries and materials

All the shells considered consisted of three layers. The two skins were the same thickness (t = 1 mm) and the core layer was filled with a material which was generally weaker than the skin. Three core layers with thicknesses e equal to 1, 9 and 49 mm, respectively (making their overall thicknesses equal to 3, 11 and 51 mm) are examined. The chosen generic geometries and the properties of the materials, which were assumed to be isotropic, are defined below:

The half-sphere

The half-sphere had a radius R equal to 1 m and was fixed at the base.

The cones

Three types of cones, with angles 30°, 45° and 60° from the horizontal, were studied. All three had the same radius at the base R_{min} equal to 1 m and the same maximum radius R_{max} equal to 2 m. The bases were fixed. Thus, 9 cases under internal pressure and 9 cases under external pressure were studied.

The materials

The materials were assumed to be elastic or perfectly elastic-plastic. The yield strain was 0.001. The same Poisson's coefficient is chosen for all materials (equal to 0.3). The Young's

modulus of the skins was $E_{skin} = 200{,}000$ MPa. For the core layer of the sandwich shells, decreasing values of the Young's modulus were chosen among the following list: $E_{core} =$ 200,000 MPa, 20,000 MPa, 2,000 MPa, 200 MPa and 20 MPa. For the nonlinear analyses, the moduli $E_{core} = 200{,}000$ MPa, 2,000 MPa and 20 MPa alone were studied. Hereafter, the ratio $\frac{E_{core}}{E_{skin}}$ will be denoted β.

The finite element models

All these cases were modeled as axisymmetric problems in two ways. The first model will be referred to as the COQMULT model. The mid-line was meshed using p + 1 nodes, *i.e.* p elements. Each layer was assumed to have its own offset, its own thickness and its own material. The second model will be referred to as the QUA8 model. The thickness was represented by 3 quadrangular isoparametric elements with 8 nodes and 9 integration points. The generatrix was meshed using q elements. Thus, the final mesh contained 3q elements and $10q + 7$ nodes. The stability analysis was carried out in the Fourier basis by seeking the Fourier mode leading to the lowest critical load.

In the case of the QUA8 mesh of the cone, rectangular elements were chosen. Thus, the mesh represented the shell's geometry exactly. A preliminary convergence study was performed for each model in order to predict the linear buckling pressure of a single layer under external or internal pressure. This study enabled us to choose the mesh size for each case. The coarsest mesh which enabled the critical pressure to converge to within 1% of the exact solution has been chosen. A decomposition into 100 regular elements along the mid-line ensured the convergence of the elastic buckling load.

Regarding the meshing of the cone, 50 shell elements were sufficient to achieve convergence. Table 1 summarizes the meshes which were chosen for the calculations.

Linear elastic buckling

Now let us compare the linear elastic buckling loads which were obtained for each case.

A formula for calculating the change in critical pressure for each case when replacing a homogenous shell by a sandwich shell

A simple method for predicting the buckling pressure of a sandwich shell modeled using shell theory if one knows the result for a shell of the same geometry, but made of a single material whose properties are those of the skin will be presented. Let us compare the membrane and bending stiffnesses of the simple shell with those of the sandwich shell. The membrane stiffness of a shell of thickness h and Young's modulus E is (Eh). The associated bending stiffness is $D = E\frac{h^3}{12(1-\nu^2)}$. Let $(Eh)^*$ and D^* denote respectively the homogenized membrane and bending stiffnesses of the multilayer shell. All the formulas giving the theoretical critical loads of the shells considered here are proportional to the product of these two stiffnesses raised to some power m:

$$k = \left(D^*(Eh)^*\right)^m \tag{27}$$

Table 1 The meshes chosen for the sphere and cone cases

Geometry	p COQMULT	q QUA8
Sphere	100	100
Cone	50	100

The ratio of the two critical loads can be expressed in general form as:

$$r_{gen} = \left(\frac{D^*(Eh)^*}{DEh} \right)^m \tag{28}$$

Now let us define the variable $x = \frac{2t}{e}$ where t is the skin thickness and e the core thickness. One has the relation $h = e\,(1 + x)$. With these notations, one has:

$$(Eh)^* = eE_{skin}\,(\beta + x) \tag{29}$$

$$D^* = e^3 \frac{E_{skin}}{12\left(1 - \nu^2\right)} \left[\beta + x\left(3 + 3x + x^2\right)\right] \tag{30}$$

Therefore, the buckling load of the sandwich shell is obtained by multiplying the critical load of the homogenous shell with the same overall thickness by the coefficient r given by the equation:

$$r = \frac{f_{case}\,(\beta, x)}{(1 + x)^m} \tag{31}$$

The function f and the power m depend on the case being considered. Here, one has three cases:

- The sphere under external pressure. The critical buckling pressure is given by the formula:

$$P_E^{sphere} = \frac{2E}{\sqrt{3\left(1 - \nu^2\right)}} \left(\frac{h}{R}\right)^2 \tag{32}$$

This critical load is found by applying the Volmir method [20], based on Donnell's shell model. The equation giving the stability of a sphere of radius R and thickness h made of a single material (Young's modulus E, Poisson's coefficient ν) under an external pressure p is:

$$D\nabla^6 w + p\frac{R}{2}\nabla^4 w + \frac{Eh}{R^2}\nabla^2 w = 0 \tag{33}$$

In Equation (33), w is the displacement normal to the shell. The solution is found by assuming that the buckling mode w satisfies $\nabla^2 w = -z^2 w$, where z is a parameter to be determined. Then, one has the following equation in w:

$$\left(Dz^4 + p\frac{R}{2}z^2 + \frac{Eh}{R^2}\right) z^2 w = 0 \tag{34}$$

Equation 34 is satisfied if the pressure p satisfies:

$$p = \frac{2Eh}{R^3 z^2} + \frac{2D}{R}z^2 \tag{35}$$

The buckling pressure is obtained for the value of z^2 which minimizes that function. One gets:

$$z_{min}^2 = \sqrt{\frac{Eh}{DR^2}} = \frac{1}{Rh}\sqrt{12\left(1 - \nu^2\right)} \tag{36}$$

Substituting z given by Equation 36 into Equation 35, one retrieves Equation 32.
Now let us extend this analytical solution to the case of multilayer spherical shells, which will enable us to predict the analytical critical pressure of the sphere under the assumption that that shell still satisfies shell theory. In order to do that, one replaces the membrane and bending stiffnesses Eh and D in Equation (33) by their homogenized values $(Eh)^*$ and D^*. Hence:

$$p^*_{crit} = \frac{4}{R^2}\sqrt{D^*\,(Eh)^*} \tag{37}$$

This is a very general formula which is valid for any kind of multilayer shell. One can immediately note that the exponent m of interest is equal to $\frac{1}{2}$.
In our case, one gets:

$$r_{sphere}\,(\beta, x) = \frac{\sqrt{\beta^2 + \beta x\left(4 + 3x + x^2\right) + x^2\left(3 + 3x + x^2\right)}}{(1+x)^2} \tag{38}$$

Now let us describe some properties of this ratio. When the Young's modulus of the core layer tends toward zero (the modular ratio of core to skin β is then 0.), the limit of the ratio r_{sphere} is:

$$r_{sphere}\,(0, x) = \frac{x\sqrt{3 + 3x + x^2}}{(1+x)^2} \tag{39}$$

When $\beta = 1$ one gets back to r = 1.

- The cone under external pressure. The buckling mode of the cone under external pressure fixed along its smaller diameter and free along its larger diameter is similar to that of a cylinder of finite length under external pressure. The proof which leads to the critical loads shows that the buckling pressure is proportional to $\left[(D^*)^3\,(Eh)^*\right]^{2.5}$. After some calculations, the ratio of the critical loads is found to be:

$$r_{cone-pext}\,(\beta, x) = \frac{\left[\left(\beta + x\left[3 + 3x + x^2\right]\right)^3\,(\beta + x)\right]^{0.25}}{(1+x)^{2.5}} \tag{40}$$

Here, the exponent m is equal to $\frac{5}{2}$. Indeed, one can note that if $\beta = 1$, $r = 1$. If β equals zero, one gets the lower critical pressure from the equation:

$$r_{cone-pext}\,(0, x) = \frac{\sqrt{x}\left(3 + 3x + x^2\right)^{\frac{3}{4}}}{(1+x)^{2.5}} \tag{41}$$

- The cone under internal pressure. In the case of the cone under internal pressure, the critical pressures are estimated by replacing the cone by an equivalent cylinder subjected to uniform axial compression at its base. The proof of the theoretical formulas giving the critical load of the cylinder [12] is more complex than, but similar to that given above for the sphere under external pressure. One can show that the critical load is still governed by $\sqrt{D^*(Eh)^*}$. Therefore, this case is similar to that of the sphere under external pressure and the reduction factor is the same:

$$r_{cone-pint}\,(\beta, x) = r_{sphere}\,(\beta, x) \tag{42}$$

The sphere under external pressure

The results of the two finite element models are compared to the values predicted by Equation (32) in Table 2 below.

Table 2 The calculated buckling loads for the 3 thicknesses

Overall thickness mm	P_E (Koiter) (MPa)	COQMULT (MPa)	QUA8 (MPa)
3	2.179	2.179	2.179
11	29.29	29.12	29.01
51	630	612	587

The agreement was very good for the two thinnest shells. The results of the calculation for the thickest shell were still close to the theoretical formula, but less accurate. Let us observe that the thicker the shell, the further the result given by the solid finite element calculation from that given by the COQMULT calculation. The latter also departed from the theoretical solution obtained with Sanders Donnell's simplified shell theory. Let us note that in the case of the thick shell the slenderness ratio ($\frac{R}{h}$) was only 20: the shell was not really thin and thin shell assumptions were no longer relevant.

Table 3 below compares, for each case, the critical pressures obtained with the two models. In all the calculations, the critical loads of Fourier modes 0 to 5 differed by less than 3%.

The calculated critical loads are given in relation to the elastic buckling load of the shell made of a single material with Young's modulus 200,000 MPa.

The analytical formula giving the critical pressure of the sandwich shell was perfectly satisfied by the multilayer shell calculation. However, the "QUA8" calculation, which is not based on the same shell assumptions, led to smaller critical pressures when the modulus of the core layer was less than, or equal to, one hundredth of the modulus of the skin. This overestimation became higher as the core layer became thicker and its stiffness became smaller.

Table 3 Sphere under external pressure: the calculated buckling loads for the different cases

Overall thickness (mm)	β	COQMULT $\frac{P_{cr}}{P^{E=200000}_{euler}}$	r_{sphere} solution	QUA8 $\frac{P_{cr}}{P^{E=200000}_{euler}}$	Ratio QUA8/ COQMULT
3	0.0001	0.80	0.80	0.022	0.30
3	0.001	0.80	0.80	0.0	0.56
3	0.01	0.80	0.80	0.256	0.94
3	0.1	0.82	0.82	0.82	0.99
3	1.	1.00	1.0	1.00	1.00
11	0.0001	0.286	0.286	0.022	0.078
11	0.001	0.286	0.286	0.073	0.25
11	0.01	0.294	0.294	0.257	0.87
11	0.1	0.364	0.364	0.369	0.98
11	1.	1.00	1.0	1.00	0.996
51	0.0001	0.065	0.065	0.0015	0.023
51	0.001	0.066	0.066	0.0092	0.13
51	0.01	0.075	0.075	0.066	0.85
51	0.1	0.160	0.160	0.165	0.97
51	1.	1.00	1.0	1.00	0.96

Figure 3 compares the critical loads obtained for all the cases with the two models. One can clearly see that both models led to the same buckling loads as long as the modulus of the core layer remained greater than one tenth that of the skins.

With the COQMULT model, once the modulus became smaller than one hundredth that of the skins, the core layer ceased to contribute to the buckling strength. Nevertheless, the critical load thus estimated still could be much greater than that obtained using a QUA8 model, which allows the two skins to have independent kinematics.

Figures (4A) and (4B) show two typical deformed shapes obtained using the COQMULT models.

In the case of the thicker shell with the smaller modulus, the critical load was overestimated by a factor of 50 when using the multilayer shell model, which is considerable. The reason was that in the case of the COQMULT model the predicted mode was such that the two skins were interdependent (Figure 4A), whereas with the QUA8 model the predicted buckling mode involved both skins when $\beta = 1$, but only the external skin when $\beta < 0.01$. This is clearly visible if one compares Figures (4C) and (4D).

The critical load of the skin alone can be obtained using Koiter's formula (Equation 32). In our case, one gets 0.242 MPa. One can observe that the lower the modulus of the core

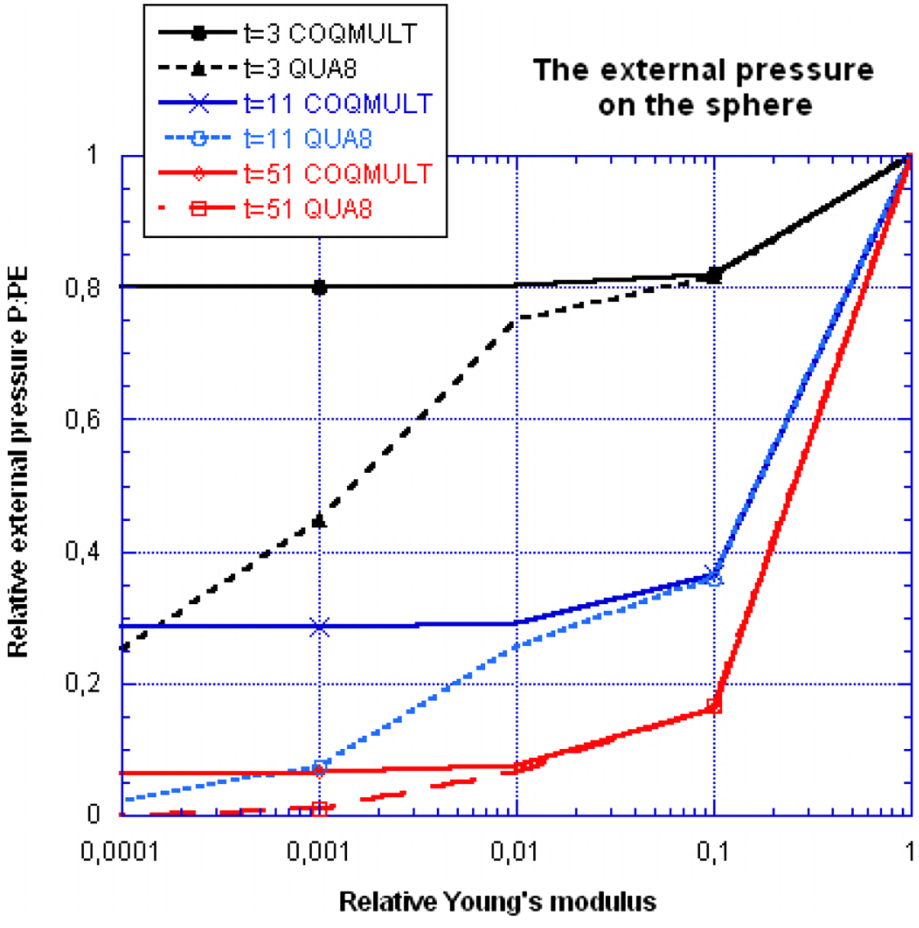

Figure 3 Comparison of the effects of the Young's modulus of the core layer on the sphere's buckling pressure using the two models (COQMULT and QUA8).

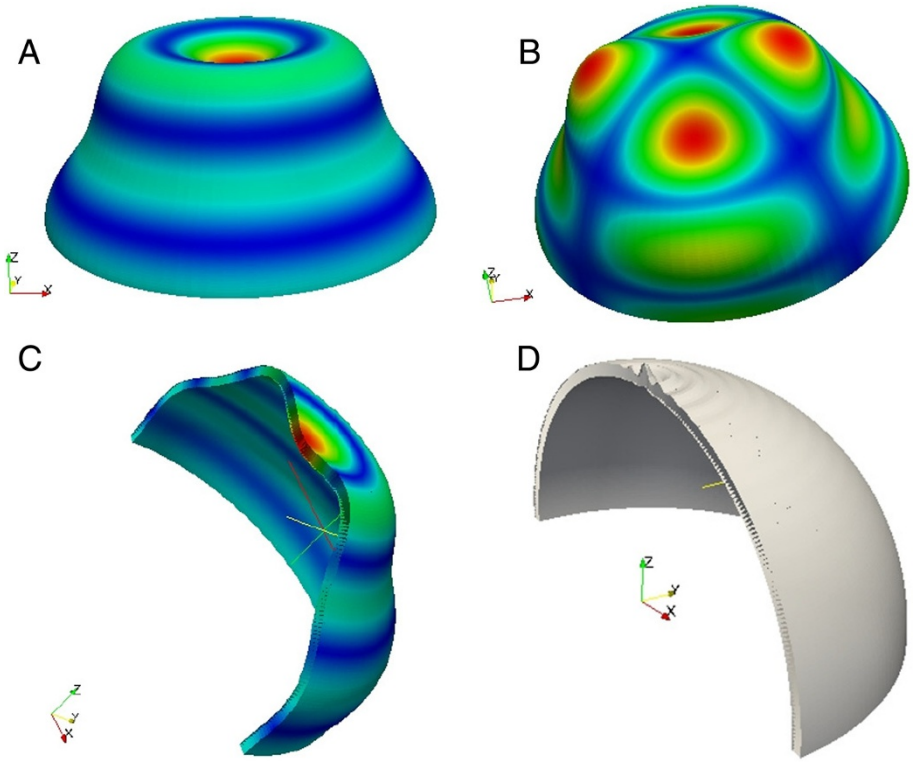

Figure 4 Comparison of the buckling modes for the 51 mm-thick sphere under external pressure. **(A)** Buckling Mode 0 (COQMULT), **(B)** Buckling Mode 2 (COQMULT), **(C)** Buckling Mode 0, $\beta = 1$ (QUA8), **(D)** Buckling Mode 0, $\beta = 0.0001$ (QUA8).

layer, the closer the critical load was to that value. Table 4 shows a comparison between the critical pressure of the skin alone and the critical pressure of the three stacked layers in the case where the modulus of the core layer was nearly zero (0.2 MPa): one can see that the critical pressure of the assembly was practically equal to that of the external skin alone in the case of the thickest shell and was 10% greater in the case of the thin shell.

The multilayer model overestimated the critical bucking load of the assembly by a factor of 100 in the case of the thickest shell, which is considerable.

The same comparison for the smallest Young's modulus of the parametric analysis ($\beta = 0.0001$) is shown in Table 5. The trend was the same, but one can see that the core layer still helped the external skin resist buckling. Nevertheless, the multilayer shell model overestimated the critical load by a factor of 3 in the case of the thin shell $\left(\frac{R}{t} = 333\right)$. This overestimation rose to a factor of 45 when the slenderness ratio was equal to 20 $\left(\frac{R}{t} = 20\right)$.

Table 4 The elastic buckling loads for $E_{core} = 0.2$ MPa

Overall thickness mm	P_{lin}^{buck} (skin) (MPa)	COQMULT (MPa)	QUA8 (MPa)
3	0.242	1.74	0.316
11	0.242	8.34	0.270
51	0.242	39.7	0.246

Table 5 The elastic buckling loads for $E_{core} = 20$ MPa

Overall thickness mm	P_{lin}^{buck} (skin) (MPa)	COQMULT (MPa)	QUA8 (MPa)
3	0.242	1.74	0.55
11	0.242	8.34	0.65
51	0.242	39.7	0.9

The cones under external pressure

Usually, cones which are fixed along their base and whose fixed radius is smaller than the free radius buckle following a non-axisymmetric mode which will be called a "skirt mode". The associated displacement is maximal on the cone's free edge. A typical mode is shown in Figure (5).

- Let us first consider the cones meshed with QUA8 elements. In order to do that, the critical loads obtained with two different representations of the same mid-line will be compared. By meshing the cones with a horizontal free boundary ("HORI") instead of a free surface perpendicular to the the mean surface ("ORTHO") (Figure 6), the buckling pressure could be reduced significantly.
  A comparison of the two buckling modes corresponding to the two meshes of the 30° cone is shown in Figure 7. One can see that the smaller critical load obtained for the model with the horizontal free surface was due to a loss of stiffness at the top of the cone, leading to a smaller buckling load.
  Table 6 shows the results in the case of the thick cone (overall thickness 51 mm, single material), for which the difference was the greatest. One can note that for the 30° angle the model with the horizontal free surface led to a critical load which was six times smaller.
  From here on, the QUA8 mesh which conforms to the geometry of the COQMULT mesh will be retained.
- Now let us compare the results of the COQMULT models with the results of the QUA8 models. Table 7 shows the results of the calculations in the case of single-material cones. Again, in this case, one can see that the critical load obtained with the solid model was very close to that given by the shell model for the two thinnest walls, and was slightly smaller for the thickest wall. Once again, the problem lies near the limit of validity of the shell model.
  The typical buckling modes of the 60° and 30° cones are shown in Figure (5).

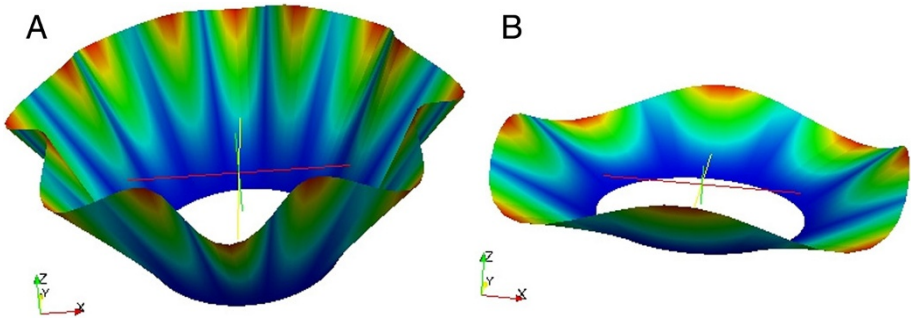

Figure 5 The typical buckling modes for two cones under external pressure. (A) "ORTHO" Mesh, **(B)** "HORI" Mesh.

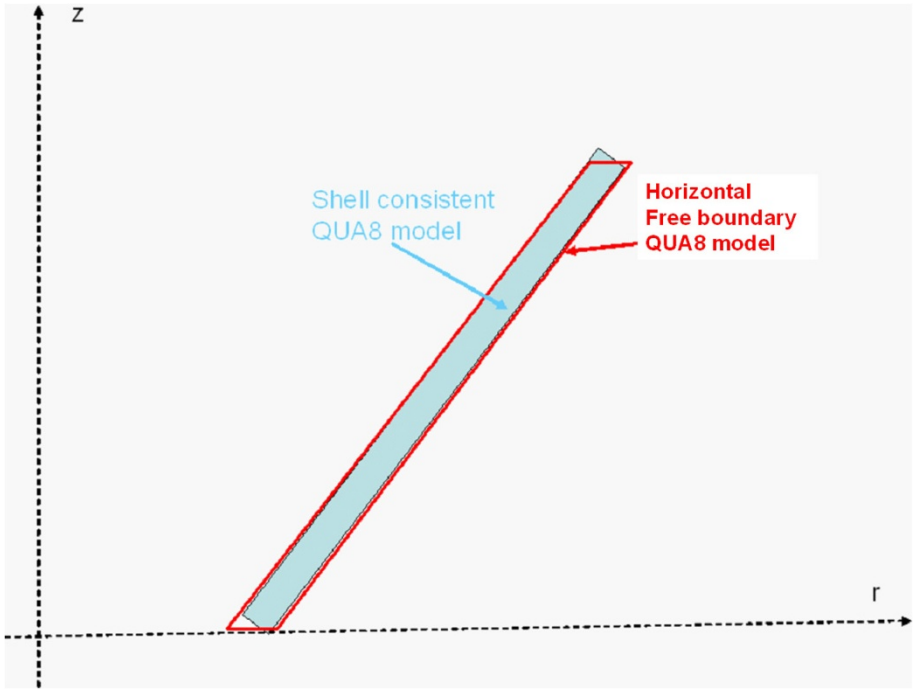

Figure 6 Schematic view of the two representations of a cone's geometry.

Tables 8, 9 and 10 show the normalized Euler loads calculated for the 9 cases and for each of the 3 cone angles studied. The last column also shows the ratio of the elastic buckling load predicted by the QUA8 model to that predicted by the COQMULT model. The agreement between the buckling pressures predicted by the COQMULT and QUA8 models was good for the two thinnest cones as long as $\beta \geq 0.01$. In the case when $\beta = 0.0001$, the critical load given by the shell model was overestimated by 30%. For the thickest cone, the critical load was overestimated by a factor of 3 to 5. Once again, the shell model precluded the buckling of the external skin alone. One can also note that when the Young's modulus of the core layer was very small the rank of the Fourier buckling mode found by the QUA8 model was always greater than that of the COQMULT model. For all the cone angles considered, the results in terms of relative pressure were quite similar, which indicates that the cone angle had very little influence on the relative loss of stiffness induced by a core layer with a smaller modulus. This can probably be explained by the facts that the mode

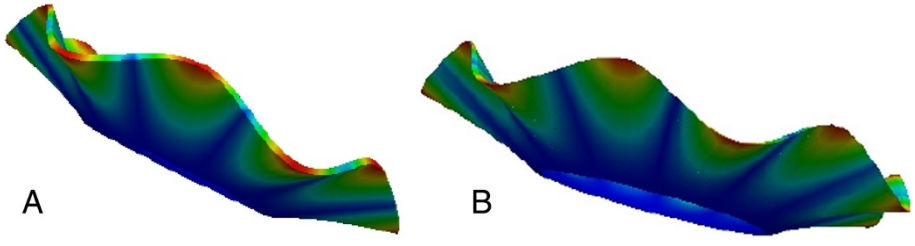

Figure 7 Comparison of the buckling modes for the 51 mm-thick 30° cone under external pressure. **(A)** 60° angle, **(B)** 30° angle.

Table 6 The calculated buckling pressures and modes for the 3 cone angles and the 3 models: Shell, QUA8 with the standard free surface ("ORTHO") and QUA8 with the horizontal free surface ("HORI")

Angle	COQMULT	Mode	Standard QUA8	Mode	Horizontal QUA8	Mode
°	(MPa)		(MPa)		(MPa)	
30	7.34	4	7.28	4	1.15	5
45	9.21	4	9.06	4	3.607	5
60	7.83	4	8.08	4	5.529	4

developed in the cone's upper portion alone and that the external radius was the same for all the shells. Finally, let us note that the estimated reduction in the critical load proposed by Formula (40) was relatively accurate for the multilayer shell model, but it overestimated the critical pressure when the modulus of the core layer was very small because it is based on a pure shell kinematics.

Figure 8 compares the effects of the stiffness of the core layer on the critical buckling mode for the two models and the three types of cones (with overall thicknesses equal to 3, 11 and 51 mm). One can observe that the behavior was very similar for each of the cone geometries and was also similar to the case of the sphere. The estimate of the reduction in the critical load given by the analytical formula remained quite acceptable. The maximum error was less than 3%.

The cones under internal pressure

The same examples were calculated with an internal pressure load. In such a case, the cone buckles following an axisymmetric mode near the smaller radius. The results for the 60°, 45° and 30° cones are given in Tables 11, 12 and 13 respectively. Once again, one can observe that the multilayer shell model drastically overestimated the critical loads when the Young's modulus of the core layer was small. In this case, the overestimation could become considerable, reaching a factor of 50 in the case of the 45° angle and the thickest shell. The ratio of the critical pressure of the single-material shell to that of the three-layer shell still followed Equation 42 as was the case for the sphere under external pressure.

Table 7 The calculated linear external buckling pressure for the 3 cone angles and the 3 thicknesses

Angle	Overall thickness	COQMULT	Mode	QUA8	Mode
°	mm	(MPa)		(MPa)	
30	3	0.0052	9	0.0052	9
30	11	0.139	6	0.139	6
30	51	7.34	4	7.28	4
45	3	0.00709	9	0.00708	8
45	11	0.187	6	0.187	6
45	51	9.21	4	9.06	5
60	3	0.00677	8	0.00678	8
60	11	0.107	6	0.108	6
60	51	7.83	4	8.08	4

Table 8 The calculated normalized external buckling pressure for the 60° cone

Overall thickness (mm)	β	COQMULT $\frac{P_{cr}}{P^{E=200000}_{COQMULT}}$	$r_{cone-pext}$	Mode	QUA8 $\frac{P_{cr}}{P^{E=200000}_{QUA8}}$	Mode	Ratio QUA8/ COQMULT
3	0.0001	0.889	0.878	8	0.729	8	0.82
3	0.001	0.889	0.878	8	0.868	8	0.98
3	0.01	0.891	0.879	8	0.888	8	1.0
3	0.1	0.899	0.892	8	0.900	8	1.0
3	1.0	1.	1.	8	1.0	8	1.0
11	0.0001	0.366	0.360	5	0.176	7	0.49
11	0.001	0.366	0.361	5	0.325	5	0.91
11	0.01	0.376	0.367	5	0.358	5	0.98
11	0.1	0.443	0.411	5	0.429	5	0.99
11	1.0	1.	1.	6	1.	5	1.02
51	0.0001	0.097	0.087	3	0.022	6	0.24
51	0.001	0.098	0.088	3	0.072	4	0.76
51	0.01	0.11	0.097	3	0.101	4	0.95
51	0.1	0.196	0.183	4	0.187	4	0.99
51	1.0	1.	1.	4	1.	4	1.03

The evolutions of the relative critical pressures as functions of β, the ratio of the moduli, are shown in Figure 9. Again, the cone angle did not appear to have much influence.

The three buckling modes are shown in Figure 10. For all the cases, one can note the presence of an axisymmetric axial compression buckling mode at the base.

Table 9 The calculated normalized external buckling pressure for the 45° cone

Overall thickness (mm)	β	COQMULT $\frac{P_{cr}}{P^{E=200000}_{COQMULT}}$	$r_{cone-pext}$	Mode	QUA8 $\frac{P_{cr}}{P^{E=200000}_{QUA8}}$	Mode	Ratio QUA8/ COQMULT
3	0.0001	0.889	0.878	9	0.698	9	0.98
3	0.001	0.889	0.878	9	0.863	9	0.97
3	0.01	0.891	0.879	9	0.890	9	1.0
3	0.1	0.900	0.892	9	0.900	9	1.0
3	1.0	1.	1.	9	1.0	8	1.0
11	0.0001	0.360	0.360	6	0.152	8	0.42
11	0.001	0.361	0.361	6	0.316	6	0.87
11	0.01	0.367	0.367	6	0.361	6	0.98
11	0.1	0.412	0.430	6	0.425	6	1.03
11	1.0	1.	1.	6	1.	6	1.0
51	0.0001	0.089	0.087	4	0.017	4	0.19
51	0.001	0.090	0.088	4	0.066	4	0.72
51	0.01	0.099	0.097	4	0.095	4	0.94
51	0.1	0.143	0.183	4	0.151	4	1.03
51	1.0	1.	1.	4	1.	5	1.0

Table 10 The calculated normalized external buckling pressure for the 30° cone

Overall thickness (mm)	β	COQMULT $\frac{P_{cr}}{P^{E=200000}_{COQMULT}}$	$r_{cone-pext}$	Mode	QUA8 $\frac{P_{cr}}{P^{E=200000}_{QUA8}}$	Mode	Ratio QUA8/ COQMULT
3	0.0001	0.890	0.878	9	0.69	9	0.78
3	0.001	0.890	0.878	9	0.86	9	0.97
3	0.01	0.890	0.879	9	0.89	9	0.99
3	0.1	0.900	0.892	9	0.900	9	1.0
3	1.0	1.	1.	9	1.0	9	1.0
11	0.0001	0.360	0.360	6	0.150	8	0.41
11	0.001	0.364	0.361	6	0.314	6	0.86
11	0.01	0.370	0.367	6	0.362	6	0.97
11	0.1	0.430	0.43	6	0.423	6	1.0
11	1.0	1.	1.	6	1.	6	1.0
51	0.0001	0.096	0.087	4	0.016	9	0.16
51	0.001	0.096	0.088	4	0.067	4	0.69
51	0.01	0.104	0.097	4	0.098	4	0.93
51	0.1	0.185	0.183	4	0.184	4	0.98
51	1.0	1.	1.	4	1.	4	0.99

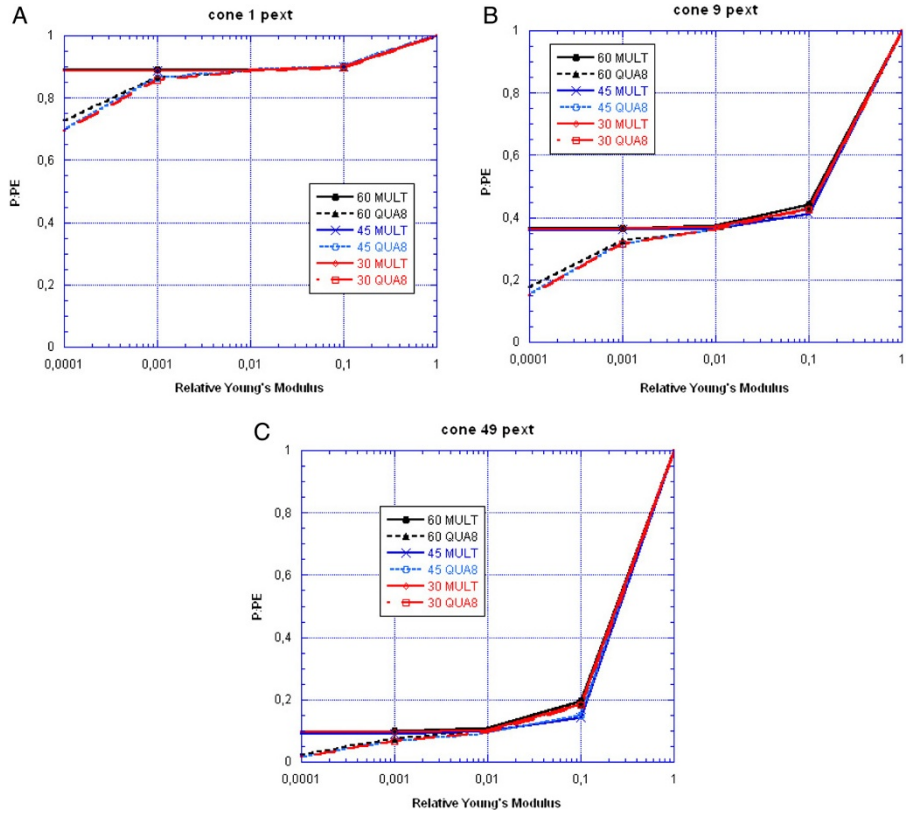

Figure 8 The effect of β (the relative stiffness of the internal layer) on the external buckling pressure of the cone. (A) Overall thickness 3 mm, **(B)** Overall thickness 11 mm, **(C)** Overall thickness 51 mm.

Table 11 The calculated relative internal buckling pressure for the 60° cone

Overall thickness (mm)	β	COQMULT $\frac{P_{cr}}{P^{E=200000}_{COQMULT}}$	$r_{cone-pint}$	QUA8 $\frac{P_{cr}}{P^{E=200000}_{QUA8}}$	Ratio QUA8/ COQMULT
3	0.0001	0.804	0.801	0.253	0.32
3	0.001	0.809	0.801	0.452	0.58
3	0.01	0.811	0.803	0.755	0.94
3	0.1	0.829	0.823	0.820	1.00
3	1.0	1.	1.0	1.	1.01
11	0.0001	0.300	0.287	0.021	0.07
11	0.001	0.300	0.287	0.072	0.24
11	0.01	0.307	0.295	0.264	0.86
11	0.1	0.377	0.365	0.371	0.98
11	1.0	1.	1.	1.0	1.0
51	0.0001	0.074	0.067	0.0015	0.02
51	0.001	0.075	0.068	0.0074	0.10
51	0.01	0.084	0.077	0.049	0.57
51	0.1	0.171	0.165	0.167	0.97
51	1.0	1.	1.	1.0	0.99

Geometrically non linear elastic-plastic buckling

The objective of this section is to answer the question: "Are the limitations of the multi-layer shell modeling of sandwich shells observed in the linear case still valid if one takes into account material and geometric nonlinearities?" In order to do that, elastic-plastic buckling was predicted by applying the method described previously to the calculation of the stability of the nonlinear elastic-plastic solution. A perfect elastic-plastic material which becomes plastic when the strain exceeds 0.001 is assumed.

Table 12 The calculated relative internal buckling pressure for the 45° cone

Overall thickness (mm)	β	COQMULT $\frac{P_{cr}}{P^{E=200000}_{COQMULT}}$	$r_{cone-pint}$	QUA8 $\frac{P_{cr}}{P^{E=200000}_{QUA8}}$	Ratio QUA8/ COQMULT
3	0.0001	0.813	0.801	0.25	0.31
3	0.001	0.813	0.801	0.49	0.60
3	0.01	0.815	0.803	0.77	0.95
3	0.1	0.833	0.823	0.83	1.00
3	1.0	1.	1.	1.0	1.00
11	0.0001	0.306	0.287	0.021	0.07
11	0.001	0.306	0.287	0.079	0.26
11	0.01	0.314	0.295	0.273	0.87
11	0.1	0.382	0.365	0.378	0.99
11	1.0	1.	1.	1.0	1.0
51	0.0001	0.078	0.067	0.0015	0.02
51	0.001	0.079	0.068	0.0067	0.08
51	0.01	0.089	0.077	0.0407	0.45
51	0.1	0.174	0.165	0.17	0.97
51	1.0	1.	1.	1.0	0.99

Table 13 The calculated relative internal buckling pressure for the 30° cone

Overall thickness (mm)	β	COQMULT $\frac{P_{cr}}{P^{E=200000}_{COQMULT}}$	$r_{cone-pint}$	QUA8 $\frac{P_{cr}}{P^{E=200000}_{QUA8}}$	Ratio QUA8/ COQMULT
3	0.0001	0.82	0.801	0.26	0.31
3	0.001	0.82	0.801	0.54	0.67
3	0.01	0.82	0.803	0.79	0.96
3	0.1	0.83	0.823	0.83	1.00
3	1.0	1.	1.0	1.	1.00
11	0.0001	0.313	0.287	0.022	0.07
11	0.001	0.314	0.287	0.097	0.31
11	0.01	0.321	0.295	0.287	0.89
11	0.1	0.389	0.365	0.385	0.99
11	1.0	1.	1.0	1.	1.00
51	0.0001	0.068	0.067	0.0017	0.026
51	0.001	0.069	0.068	0.0072	0.10
51	0.01	0.078	0.077	0.044	0.57
51	0.1	0.160	0.0165	0.162	1.00
51	1.0	1.	1.0	1.	1.01

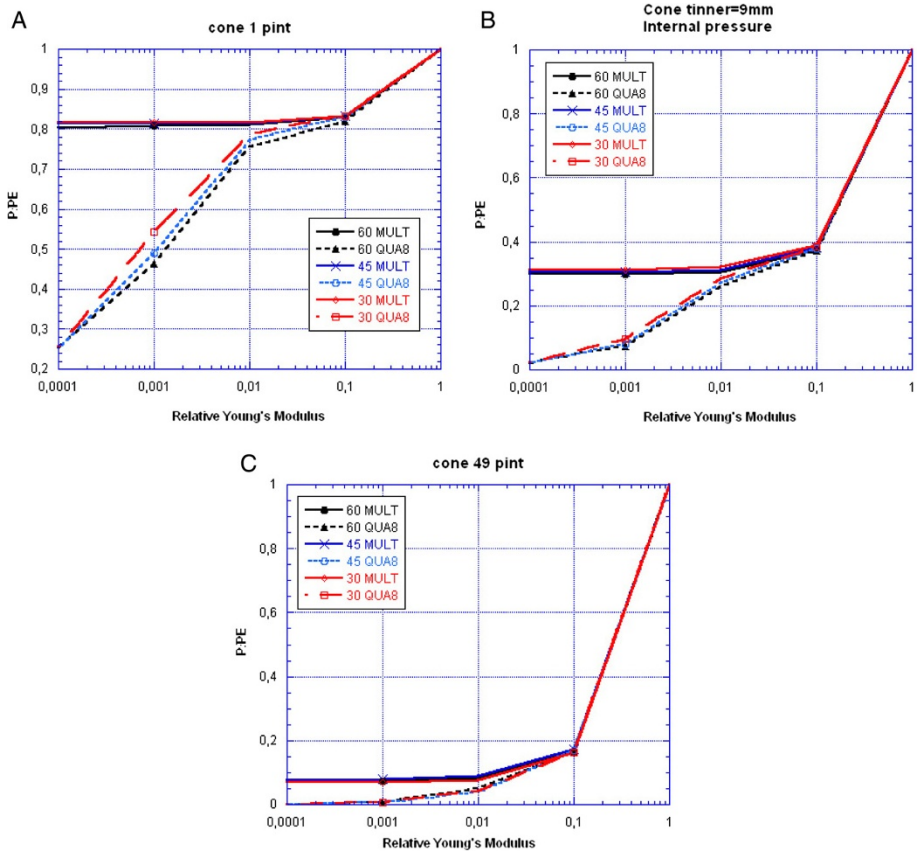

Figure 9 The effect of β (the relative stiffness of the core layer) on the cone's internal buckling pressure. (A) Overall thickness 3 mm, **(B)** Overall thickness 11 mm, **(C)** Overall thickness 51 mm.

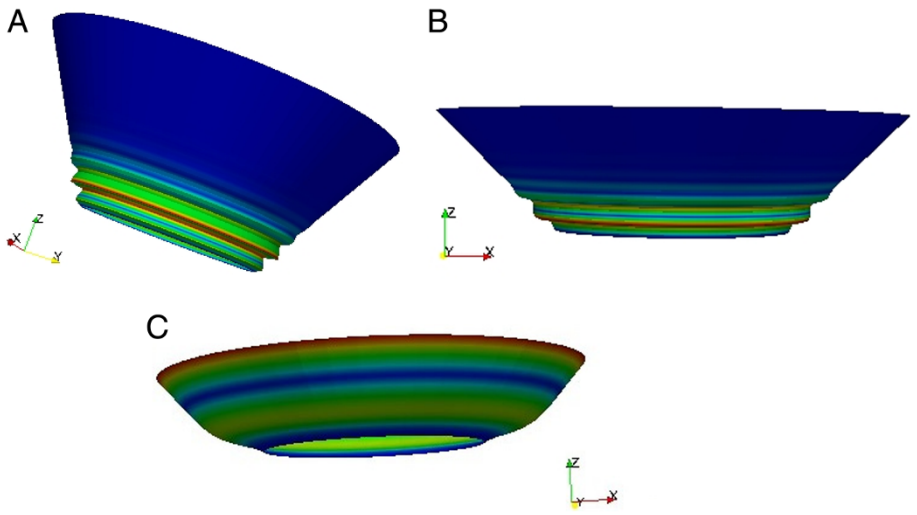

Figure 10 The buckling modes of the cones under internal pressure. (A) 60° angle, **(B)** 45° angle, **(C)** 30° angle.

The sphere under external pressure

- First, the nonlinear stability analysis was carried out for all the cases.
  For the sphere under external pressure, the results shown in Table 14 were obtained. One can note that plasticity reduced the buckling load by a factor of 2 for the thinnest spheres. The elastic-plastic critical load was 50 times smaller for the thickest spheres. One observes that the multilayer model is not dependable when the modulus of the core layer is very small. Once again, the local buckling mode of the external layer alone could not be predicted. The conclusion drawn in the case of elastic buckling still holds for nonlinear buckling.
- Now let us compare the critical loads and complete incremental responses of the COQMULT and QUA8 models in the case of more significant differences. This concerns the spheres with a 49 mm-thick core layer (overall thickness 51 mm) and a modulus equal to 20 MPa. This case can be calculated relatively easily because the

Table 14 The calculated elastic-plastic buckling loads for the sphere under external pressure

Overall thickness (mm)	β	COQMULT P_{crit}^{plast} (MPa)	$\frac{P_{crit}^{plast}}{P_E}$	QUA8 P_{crit}^{plast} (MPa)	$\frac{P_{crit}^{etan}}{P_E}$	Plasticity ratio QUA8/ COQMULT
3	0.0001	0.80	0.46	0.08	0.14	0.1
3	0.01	0.8	0.46	0.77	0.47	0.96
3	1.	1.17	0.54	1.16	0.53	0.99
11	0.0001	0.80	0.096	0.095	0.148	0.12
11	0.01	0.836	0.098	0.833	0.11	1.0
11	1.	4.4	0.15	4.39	0.15	1.
51	0.0001	0.802	0.02	0.018	0.021	0.023
51	0.01	1.0	0.022	0.98	0.025	0.98
51	1.	20.4	0.033	19.8	0.034	0.97

buckling modes are axisymmetric and, thus, one does not have to carry out coupled Fourier series calculations. Thus, one can use this case to compare the post-buckling behavior given by the two models. The results are summarized in Table 15. Several effects can be observed. For the COQMULT model with no defect, the two analyses (incremental and bifurcation prediction based upon the tangent modulus theory) led to approximately similar results. In the case of the QUA8 model, the predictions achieved with the three methods – buckling using the tangent modulus (etan), buckling using incremental plasticity theory (flow) and incremental analysis – led to different results. The incremental analysis without defect overestimated the critical load by 50%, except for the case when $\beta = 0.0001$. In the other cases, the estimates of the critical loads were identical for the COQMULT and QUA8 models regardless of the bifurcation analysis performed. In the case when $\beta = 0.0001$, the multilayer shell analysis overestimated the critical load by 50% when the buckling was not estimated using tangent modulus theory.

Figure 11 shows the comparison of the displacements at the top of the sphere obtained using the two incremental calculations COQMULT and QUA8 with no defect (the case when $\beta = 0.0001$). On this curve, one can clearly see that the thickness of the shell modeled with QUA8 elements diminishes at the top, a phenomenon which cannot be accounted for by the COQMULT model. The tangent modulus model appears to lead to an overly pessimistic estimate of the critical load in the case when $\beta = 0.0001$.

Figures 11 and 12 show a comparison of the displacements at the top of the sphere given by the COQMULT model respectively without and with a variable modal amplitude defect. The post-buckling behavior appears to be stable.

The cones under external pressure

The results of the elastic-plastic bifurcation calculations are given in Tables 16, 17 and 18 below. Let us note that all the bifurcations occurred for non-axisymmetric modes and that Fourier series analysis is very efficient in such cases. The lowest mode was always Mode 3. The thickest cone with the smallest core layer modulus meshed with QUA8 elements buckled following Mode 19. Of course, such an analysis could be carried out in 3D, but this would require significantly longer computation times: indeed, one would go from 300 2D Fourier elements to several tens of thousands of 3D elements.

For the cones under external pressure, one can note that the buckling was elastic for the two thinnest configurations. For the thickest shell, the buckling was elastic-plastic. No significant nonlinear geometric effect was observed for this type of buckling. Once

Table 15 Comparison of the estimated elastic-plastic buckling loads for the 51 mm-thick sphere under external pressure

β	COQMULT		QUA8		
	P_{etan}^{plast} MPa	P_{incr}^{max} MPa	P_{etan}^{plas} MPA	P_{flow}^{plas} MPa	P_{incr}^{max} MPa
0.0001	0.802	0.803	0.018	0.555	0.56
0.01	1.0	1.07	0.98	1.02	1.42
1.	20.4	20.5	19.8	20.44	33.7

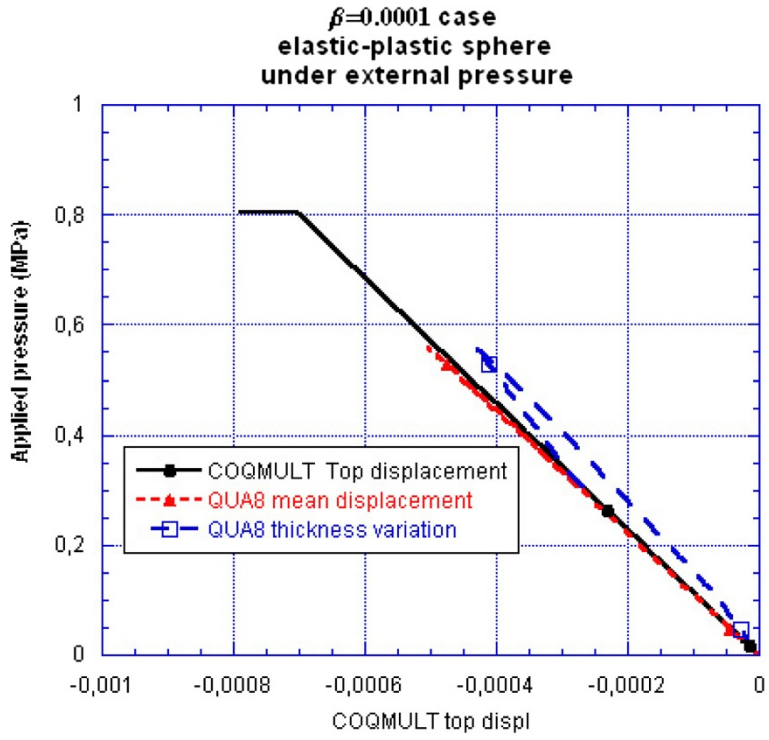

Figure 11 Comparison of the top inner displacements given by the COQMULT and QUA8 models.

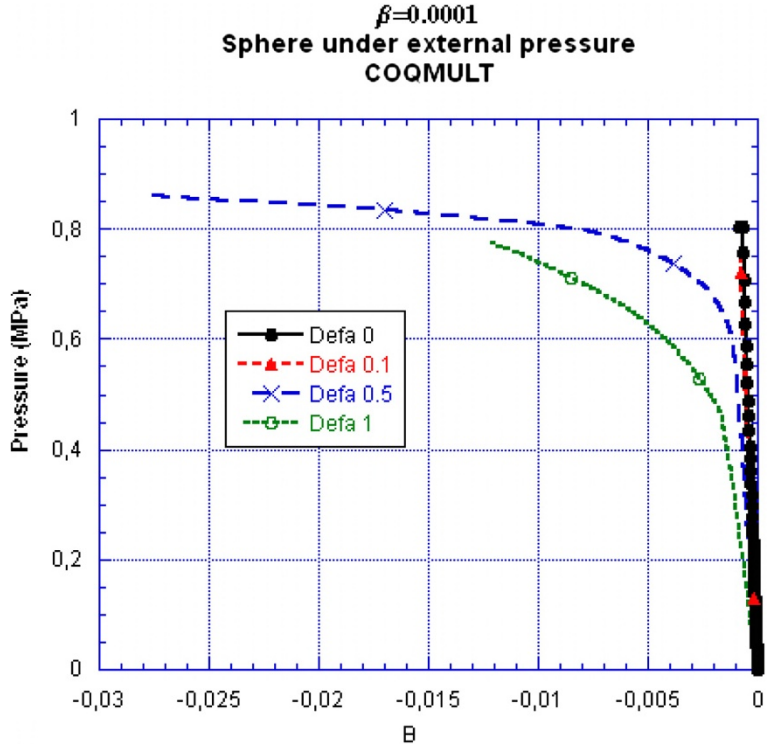

Figure 12 The effect of an initial imperfection (0, 0.01, 0.1) on the maximum pressure (COQMULT model).

Table 16 The calculated elastic-plastic buckling load under external pressure for the 60° cone

Overall thickness (mm)	β	COQMULT P_{crit}^{plast} (MPa)	$\frac{P_{crit}^{plast}}{P_E}$	QUA8 P_{crit}^{plast} (MPa)	$\frac{P_{crit}^{plast}}{P_E}$	Plasticity ratio QUA8/ COQMULT
3	0.0001	0.00605	1.0	0.00496	1.	0.82
3	0.01	0.00607	1.0	0.00605	1.	1.
3	1.	0.00859	1.27	0.00681	1.	0.79
11	0.0001	0.0627	1.0	0.028	0.9	0.44
11	0.01	0.0642	1.0	0.063	1.	0.98
11	1.	0.201	1.18	0.158	0.9	0.79
51	0.0001	0.175	0.23	0.032	0.18	0.18
51	0.01	0.219	0.25	0.196	0.24	0.89
51	1.	4.15	0.53	3.55	0.44	0.86

again, when the modulus of the core layer was very small, the buckling mode was a skin mode. This effect cannot be predicted using the COQMULT model. Because of elastic-plasticity, the thicker the cone, the smaller the ratio of elastic-plastic to elastic buckling pressure. These results confirm those obtained previously in the case of the sphere under external pressure. For the 30° case and a very low stiffness of the core layer, the critical load predicted by the elastic-plastic solid model was 10 times smaller.

The cones under internal pressure

Tables 19, 20 and 21 below show the complete results of the plastic bifurcation calculations. Let us note that all the bifurcations occurred for axisymmetric modes. These bifurcation analysis results can be compared to the results of nonlinear elastic-plastic analyses. In this case, the buckling was clearly plastic. Overall, the comparison between

Table 17 The calculated elastic-plastic buckling load under external pressure for the 45° cone

Overall thickness (mm)	β	COQMULT P_{crit}^{plast} (MPa)	$\frac{P_{crit}^{plast}}{P_E}$	QUA8 P_{crit}^{plast} (MPa)	$\frac{P_{crit}^{plast}}{P_E}$	Plasticity ratio QUA8 / COQMULT
3	0.0001	0.0063	1.0	0.00501	1.01	0.79
3	0.01	0.0063	1.0	0.00634	1.	1.0
3	1.	0.00898	1.27	0.00715	1.	0.8
11	0.0001	0.068	1.0	0.0134	0.47	0.20
11	0.01	0.069	1.0	0.068	1.	0.98
11	1.	0.212	1.13	0.188	1.	0.89
51	0.0001	0.144	0.175	0.0159	0.10	0.11
51	0.01	0.178	0.195	0.154	0.18	0.97
51	1.	9.21	0.382	2.66	0.294	0.76

Table 18 The calculated elastic-plastic buckling load under external pressure for the 30° cone

Overall thickness (mm)	β	COQMULT P_{crit}^{plast} (MPa)	$\frac{P_{crit}^{plast}}{P_E}$	QUA8 P_{crit}^{plast} (MPa)	$\frac{P_{crit}^{plast}}{P_E}$	Plasticity ratio QUA8/ COQMULT
3	0.0001	0.0046	1.0	0.0032	0.9	0.70
3	0.01	0.0046	1.0	0.0047	1.01	1.0
3	1.	0.0066	1.27	0.0054	1.04	0.82
11	0.0001	0.051	1.0	0.00708	0.37	0.15
11	0.01	0.052	1.0	0.051	1.02	0.98
11	1.	0.159	1.14	0.14	1.01	0.89
51	0.0001	0.097	0.14	0.01	0.08	0.10
51	0.01	0.12	0.16	0.104	0.15	0.87
51	0.1	2.58	0.35	1.75	0.24	0.68

the COQMULT and QUA8 models leads to the same conclusions as for elastic buckling: the COQMULT model drastically overestimated the critical load when the modulus of the core layer of the sandwich shell was very small. Again, in this case, one had a plastic buckling mode of the skin alone, which the COQMULT model is unable to predict. Depending on the case, the nonlinear elastic-plastic critical load varied between one hundredth and 90% of the elastic buckling load.

In this case, one finds again, although to a lesser degree than for the sphere, that tangent modulus theory led to a safe estimate of the critical load for $\beta = 0.0001$, the QUA8 model and the thickest shell. For the other cases, the COQMULT became more unsafe as the shell's thickness increased. The critical plastic buckling pressure predicted using incremental plasticity theory along with the QUA8 model was

Table 19 The calculated elastic-plastic buckling load under internal pressure for the 60° cone

Overall thickness (mm)	β	COQMULT P_{crit}^{plast} (MPa)	$\frac{P_{crit}^{plast}}{P_E}$	QUA8 P_{crit}^{plast} (MPa)	$\frac{P_{crit}^{plast}}{P_E}$	Plasticity ratio QUA8 / COQMULT
3	0.0001	0.156	0.3	0.0186	0.11	0.12
3	0.01	0.158	0.3	0.15	0.31	0.95
3	1.	0.307	0.48	0.224	0.35	0.73
11	0.0001	0.175	0.062	0.0306	0.15	0.18
11	0.01	0.183	0.064	0.142	0.06	0.78
11	1.	1.04	0.11	0.892	0.09	0.86
51	0.0001	0.183	0.01	0.0039	0.01	0.02
51	0.01	0.253	0.012	0.183	0.016	0.72
51	1.	4.64	0.019	3.3	0.014	0.71

Table 20 The calculated elastic-plastic buckling load under internal pressure for the 45° cone

Overall thickness (mm)	β	COQMULT P_{crit}^{plast} (MPa)	$\frac{P_{crit}^{plast}}{P_E}$	QUA8 P_{crit}^{plast} (MPa)	$\frac{P_{crit}^{plast}}{P_E}$	Plasticity ratio QUA8/ COQMULT
3	0.0001	0.127	0.35	0.04	0.37	0.33
3	0.01	0.128	0.35	0.11	0.31	0.85
3	1.	0.248	0.55	0.18	0.39	0.71
11	0.0001	0.145	0.07	0.01	0.07	0.07
11	0.01	0.152	0.07	0.12	0.06	0.79
11	1.	0.860	0.125	0.59	0.09	0.69
51	0.0001	0.145	0.01	0.006	0.02	0.04
51	0.01	0.184	0.01	0.048	0.006	0.26
51	1.	3.80	0.02	0.77	0.004	0.2

up to 50% greater than using tangent modulus theory. However, both these critical loads were always smaller than, or equal to, that obtained using the COQMULT model.

Conclusions

This paper presented the analytical formulae for the elastic buckling loads of sandwich cones and spheres under pressure loading. These formulae were successfully compared to multilayer shell calculations. Then, one showed the limitations of that formulation which relies on a shell kinematics which does not allow the skins to wrinkle independently of each other. The calculations were compared to continuum mechanics calculations, which are the most relevant calculations in these cases.

All these calculations showed that when the Young's modulus of the sandwich shell's core layer is more than one tenth that of the skins the multilayer model suffices. When the ratio of the moduli is less than one hundredth (which is often the case with foam

Table 21 The calculated elastic-plastic buckling load under internal pressure for the 30° cone

Overall thickness (mm)	β	COQMULT P_{crit}^{plast} (MPa)	$\frac{P_{crit}^{plast}}{P_E}$	QUA8 P_{crit}^{plast} (MPa)	$\frac{P_{crit}^{plast}}{P_E}$	Plasticity ratio QUA8 / COQMULT
3	0.0001	0.086	0.44	0.004	0.06	0.05
3	0.01	0.087	0.44	0.06	0.34	0.75
3	1.	0.165	0.69	0.11	0.48	0.70
11	0.0001	0.10	0.09	0.01	0.09	0.09
11	0.01	0.11	0.09	0.08	0.75	0.75
11	1.	0.61	0.16	0.39	0.64	0.64
51	0.0001	0.11	0.015	0.011	0.06	0.10
51	0.01	0.13	0.016	0.095	0.02	0.71
51	0.1	2.70	0.025	1.19	0.01	0.44

materials) skin modes are likely to occur at pressures which are much lower than those predicted by the multilayer model. These conclusions are valid both in elasticity and in nonlinear elastic-plasticity. The analysis which is proposed here for the axisymmetric case is particularly efficient since a linear calculation such as those which were carried out in this study takes no more than a few seconds on a laptop PC and a nonlinear solid calculation takes only a few minutes.

Competing interests
The authors declare that they have no competing interests.

Authors' contributions
The author has programmed the software made all the computations and developements presented in this work. The article was first written in French, then translated in English by a professionnal translator.

Received: 1 March 2013 Accepted: 3 May 2013
Published: January 29, 2014

References

1. Budiansky B (1999) On the minimum weight of compression structures. Int J Solids Struct 36:3677–3708
2. Hutchinson JW, He MY (2000) Buckling of cylindrical sandwich shells with metal foam cores. Int J Solids Struct 37(46-47):6777–6794
3. Bazant Z, Beghini A (2004) Sandwich buckling formulas and applicability of standard computational algorithms for finite strains. Composites Part B Eng 35(6-8):573–581
4. Anon (1965) Buckling of thin circular cylinders. NASA Space Vehicle Design Criteria, NASA SP-8007
5. Ji W, Waas AM (2007) Global and local buckling of sandwich beams. J Engineering Mech. 230–237
6. Zhang Z, Liu S, Tang Z (2010) Crashworthiness investigation of kagome honeycomb sandwich cylindrical colums under axial crushing loads. Thin Walled Struct 48:9–18
7. Walker M, Smith M (2006) A procedure to select the best material combination and optimally design sandwich composite cylindrical shells for minimum mass. Mater Des 27(2):160–165
8. Leotoing L, Drapier S, Vautrin A (2002) First application of a novel unified model for local and global buckling of sandwich columns. Eur J Mech A/Solids 21:683–701
9. Golterman P, Molmann H (1989) Interactive buckling in thin walled beams: II applications. Int J Solids Struct 25(7):729–749
10. Molmann H, Golterman P (1989) Interactive buckling in thin walled beams: I theory. Int J Solids Struct 25(7):715–728
11. Szyniszewski S, Smith BH, Hajjar JF, Arwade SR, Schafer BW (2012) Local buckling strength of steel foam sandwich panels. Thin-Walled Struct 59:11–19
12. Koiter WT (1970) On the stability of elastic equilibrium. AFFDL-TR-70-25 Technical report
13. Bushnell D (1985) Computerized buckling analysis of shells. Springer, Series: Mech Elastic Stability 9 ISBN 978-90-247-3099-5
14. Bushnell D (1974) Bifurcation buckling of shells of revolution including large deflections, plasticity and creep. Int J Solids Struct 10:1287–1305
15. Ahmad S, Irons BM, Zienkiewicz OC (2005) Analysis of thick and thin shell structures by curved finite elements. Int J Numerical Methods Eng 2(3):419–451
16. Combescure A (1986) Static and dynamic buckling of large thin shells. Nucl Eng Des 92(3):339–354
17. Ricks E (1979) An incremental approach to the solution of snapping and buckling problems. Int J Solids Struct 15:524–551
18. Crisfield M (1980) A fast incremental-iterative solution procedure that handles snap through. Comput Struct 13:57-62
19. Gusic G, Combescure A, Jullien JF (2000) The influence of circumferential thickness variations on the buckling of cylindrical shells under external pressure. Comput Struct 74(4):461–477
20. Volmir AS (1963) Stability of elastic systems. Gos. Izd-vo Fiz.-Mat. Lit., Moscow

doi:10.1186/2213-7467-1-2
Cite this article as: Combescure: **Modeling elastic-plastic buckling of sandwich axisymmetric shells: on the limits of "shell" models and analytical solutions.** *Advanced Modeling and Simulation in Engineering Sciences* 2014 **1**:2.